Investigations on the formation mechanism of hydroxyapatite synthesized by the solvothermal method

Ying Jun Wang[1,3]**, Chen Lai**[1]**, Kun Wei**[1]**, Xiaofeng Chen**[1]**, Yong Ding**[2] **and Zhong Lin Wang**[2]

[1] Key Laboratory of Specially Function Materials and Advanced Manufacturing Technology of Ministry of Education, South China University of Technology, Wushan Road, Guangzhou 510640, Guangdong, People's Republic of China
[2] School of Materials Science and Engineering, Georgia Institute of Technology, Atlanta, GA 30332-0245, USA

E-mail: imwangyj@scut.edn.cn

Abstract

In this paper, uniform hydroxyapatite (HA) nanowires of width 60 nm and length 1 μm are synthesized by solvothermal synthesis. The formation process of the nanowires has been elaborated from the structure within the reverse micelles by the time-resolved fluorescence quenching technique. The results reveal that the formation of amorphous nuclear/surfactant complex and the electrostatic field within the reverse micelles maintain the unidirectional, irreversible fusion of reverse micelles, leading to the growth of nanowires in one direction. In the solvothermal synthesis, the pressure generated in the autoclave is estimated. The results suggest that the products are prepared under stable conditions without intense shearing stress where it is favourable for the formation of long and uniform HA nanowires.

1. Introduction

One-dimensional (1D) nano-biomaterials have stimulated great interest due to their importance in basic scientific research and potential applications in biomedical fields. Various methods have been developed for the synthesis of 1D nano-materials, including the vapour–liquid–solid process, solid–vapour process and template-based methods [1–3]. While the above research work mainly focused on semiconductors and 1D oxide systems such as Si, GaAs, ZnO and SiO_2, only several types of inorganic 1D nanomaterials such as $BaSO_4$, $BaCO_3$ and $CaSO_4$ have been synthesized by reverse micelles or microemulsions at room temperature [4–6]. Certain surfactant molecular groups all together form reverse micelles in bulk hydrophobic solvents, such as heptane and cyclohexane. The micelle has polar cores that may accommodate a large amount of water, forming a 'water pool' for nanomaterials synthesis. Reverse micelles or microemulsion is an effective approach for synthesis of 1D nanomaterials because it can create a large interface between the aqueous and nonpolar phases,

allowing reactants that prefer different phases to be brought together, thereby increasing their local concentration and hence increasing the reaction rate [7, 8]. Furthermore, reverse micelles compartmentalize reactants at the nanometre level in compartmentalized water domains, whose morphologies (spheres, rods, discs or bicontinuous) are determined to a large extent by the specific surfactant employed. The effects of Brownian motion lead to fusion–fission between reverse micelles; thereby, the reactants are exchanged and mixed and react to form the products. Various authors have proposed the hypothesis that organized surfactant molecules lead to inorganic crystal nucleation [9–12], involving the irreversible fusion, unidirectional exchange and coalescence of reverse micelle droplets. However, a general formation mechanism of nanomaterials in reverse micelles is still on the way and we need to be seeking more studies and data.

Time-resolved fluorescence quenching studies have proved to be a useful and important method to investigate the water pool within the reverse micelles [13–16]. Some molecules, which are called 'probes', exhibit spectral or lifetime changes in different micellar environments, revealing

[3] Author to whom any correspondence should be addressed.

the characters of their local surroundings. Hence, the position of the probe, which is bonded to the ionized surfactant molecules or isolated in the core of reverse micelles, will give information about the interface [13, 17] or water pool [18] in reverse micelles and the motion of probe molecules can be reflected by the fluorescence decay curves.

Hydroxyapatite, $Ca_{10}(PO_4)_6(OH)_2$(HA), is the major constituent of vertebrate bone and tooth, and some ectopic calcification [19]. In recent years, synthetic hydroxyapatite has been of substantial interest and importance because of its biocompatibility and rapid integration into the human body. Unfortunately, due to poor mechanical reliability, especially in an aqueous environment, HA bioceramics cannot be used for heavy-load-bearing applications. By using 1D HA nanomaterials to reduce the grain boundary problem, many useful and desirable properties of HA nanoparticles are not only preserved but also enhanced due to the high aspect ratio for increasing mechanical flexibility and toughness [20]. The commonly used techniques for the synthesis of HA are chemical co-precipitation, the sol–gel process and hydrothermal synthesis [21–23]. However, the morphologies of the HA particles synthesized by these methods are often spherical or needle-like with small aspect ratio. Although HA nanowires had been synthesized in the reverse microemulsion, the final products are amorphous or with low crystallization. The hydrothermal synthesis can be carried out at a relatively low reaction temperature ($<250\,°C$) to produce a sufficiently high-quality crystalline product without post-calcination. The solvothermal synthesis combines hydrothermal synthesis and reverse micelle solution, providing a unique approach for synthesis of HA nanowires. The products of solvothermal reactions are usually crystalline and do not require postannealing treatments. At the same time, the morphologies of the products can be controlled by the reverse micelles.

In previous experiments [12, 24, 25], we have presented a novel solvothermal approach by which the crystalline and high aspect ratio nanowires of calcium phosphate (one of the members of the apatite family) at large scale was synthesized. Moreover, the particle morphology and size were found to be a strong function of the water-to-surfactant molar ratio (W_0), co-surfactant-to-surfactant molar ratio (P_0), reaction temperature and time. In this paper, the pure HA nanowires are synthesized and details about the formation process of the nanowires are elaborated. To describe a generalized mechanism for the growth of HA nanowires, we investigate the 'water pool' by time-resolved fluorescence quenching techniques, using $[Ru(bpy)_3]^{2+}$ (ruthenium complex) as fluorescent probe. The solvothermal synthesis involves two steps: the first one is the nucleation process at room temperature; the second one is the growth of HA nanowires under higher temperature and pressure. The time-resolved fluorescence quenching experiment focuses on the first step in this paper. The reaction pressure is estimated to provide more information about the solvothermal synthesis in the opaque autoclave.

2. Experiments and method

2.1. Materials

Calcium nitrate ($Ca(NO_3)_2 \cdot 4H_2O$), phosphoric acid (H_3PO_4), cetyltrimethylammonium bromide (CTAB), am-

monia ($NH_3 \cdot H_2O$), n-pentanol and cyclohexane were used as received from the vendor. The ruthenium complex, $[Ru(bpy)_3]Cl_2$, was made from $RuCl_2 \cdot H_2O$ according to the procedure described by Foreman *et al* [26].

2.2. Nanowire preparation

Stock solutions of Ca^{2+} and PO_4^{3-} were prepared separately by dissolving the desired amount of $Ca(NO_3)_2 \cdot 4H_2O$ and H_3PO_4 in distilled water, forming 1 M Ca^{2+} solution and 0.5 M PO_4^{3-} solution. Then, 1.6 g CTAB and 1.6 ml n-pentanol were added to 40 ml cyclohexane with acute magnetic stirring. Then, 0.42 ml of 0.5 M PO_4^{3-}-containing solution was injected into the solution. When CTAB dissolved completely, 0.42 ml of 1 M Ca^{2+}-containing solution was then injected into the above translucent reverse solution. The mixture was under continuous stirring for 0.5 h, with modified pH value with ammonia to 7.5. The final transparent reverse solution was transferred into a sealed Teflon container and statically heated in a oven at $120\,°C$ for 12 h. After solvothermal synthesis, the inorganic component was separated at room temperature by centrifugation of the liquid reverse micelle solution at 11 000 rpm for 20 min. The resulting white precipitate was washed thoroughly with a mixture solution of ethanol and ether (volume ratio = 1:1) and oven-dried at about $50\,°C$.

2.3. Time-resolved fluorescence quenching experiment

The Ca-containing reverse micelle solution was prepared by adding Ca^{2+} solution to the CTAB containing cyclohexane and the n-pentanol, and placed on the magnetic stirrer for half an hour until a transparent isotropic solution was obtained. The same procedure was repeated to prepare the P-containing reverse micelles. Then the two reverse micelle solutions were rapidly mixed, and stirred again for half an hour until the system was transparent and uniform. To this was added an aliquot of water containing $[Ru(bpy)_3]^{2+}$ with the volume determined by the desired W_0. Surfactant to probe ratios were always $>10^3$ to avoid multiple probe occupancy. The above procedure was repeated in each process when the reactant solution was substituted by pure water.

Fluorescence intensities can be adequately fitted to exponential decay [13–16]. Monoexponential decays in the absence of quenching imply that the excited molecules constitute a single and homogeneous population, and isotropy decays can be fitted by a monoexponential as equation (1). In contrast to the isotropy decay in some case, the anisotropy decay in dispersions is fitted by a biexponential function as shown in equation (2).

$$I = I_0 \exp\left(-\frac{t}{\tau}\right) \tag{1}$$

$$I = A \exp\left(-\frac{t}{\tau_1}\right) + B \exp\left(-\frac{t}{\tau_2}\right) \tag{2}$$

where I is fluorescent intensity; I_0 is the initial fluorescent intensity; A, B are constants; t is time and τ, τ_1 and τ_2 are fluorescent lifetime.
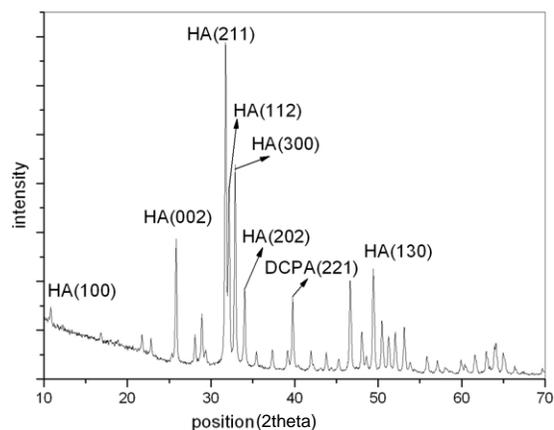
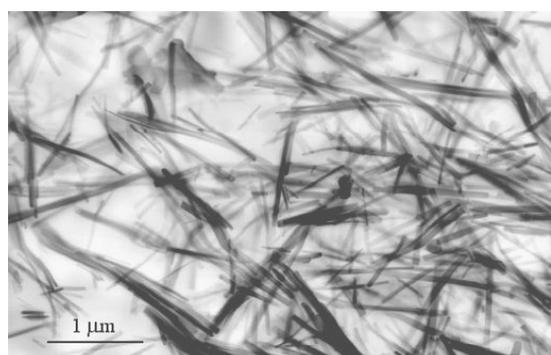**Figure 1.** XRD patterns of hydroxyapatite nanowires prepared at $W_0 = 10$, $P_0 = 3$.

Figure 2. SEM image of hydroxyapatite nanowires as prepared.

2.4. Characterization

The phase composition and crystallinity of the calcined powders were analysed using x-ray diffraction (XRD) equipped with a Brüker AXS, D8 Advance Diffractometer with Cu Kα radiation at 40 kV and 40 mA. The morphologies and structure were investigated at 400 kV using a JEOL 4000EX high-resolution transmission electron microscope. Emission spectra and decays were collected on an Edinburgh FLS 920. The lamp was operated in 0.8 bar of N$_2$, samples were excited at 272 nm and emission was selected by using 380 and 570 nm long-pass filters. The fluorescence lifetimes were determined by convoluting the instrument response with an exponential decay model using an iterative procedure to minimize the residuals.

3. Results and discussion

3.1. Structural characterization

The solvothermal synthesis is a cationic four-component reversed micelle system with the surfactant hexadecyltrimethylammonium bromide (CTAB), n-pentanol as co-surfactant and 1 M aqueous Ca(NO$_3$)$_2$ and 0.5 M H$_3$PO$_4$ solution at neutral pH in cyclohexane. We define the following quantities for characterizing the reaction: W_0 represents the molar ratio of water
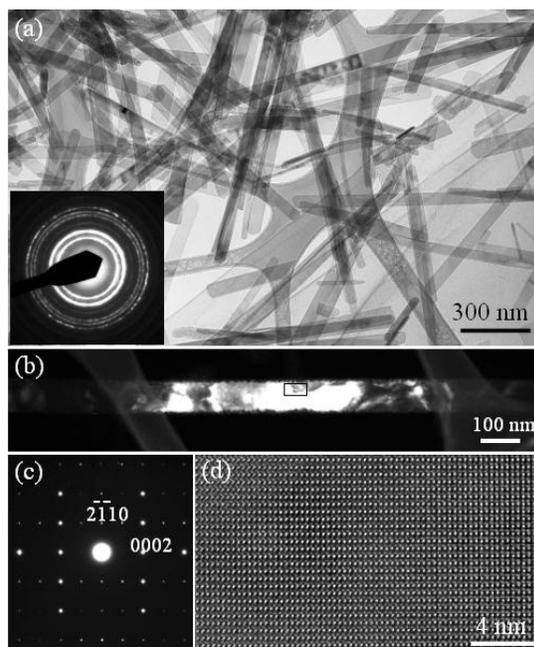

Figure 3. (a) Low-magnification TEM of the hydroxyapatite nanowires and the corresponding electron diffraction pattern recorded from dozens of randomly oriented nanowires. The sample was prepared at $W_0 = 10$, $P_0 = 3$, pH = 8.02. (b) Low-magnification dark-field TEM image, and (c) the corresponding electron diffraction.

to CTAB and P_0 the molar ratio of n-pentanol to water. At $W_0 = 10$ and $P_0 = 3$, the dominant phase is HA with minor phase DCPA (figure 1). These were the right conditions for large-scale synthesis of HA, under which the percentage of DCPA phase was very minor. The as-synthesized HA at $W_0 = 10$ and $P_0 = 3$ has one-dimensional nanowire-like morphology, as shown by the SEM image in figure 2. The lengths of the nanowires are approximately 1 μm, and their widths are quite uniform. The TEM image clearly presents the uniform morphologies of the nanowires, displaying a width of approximately 60 nm (figure 3(a)). The inset is a selected-area electron diffraction pattern corresponding to numerous nanowires in random orientation. The diffraction pattern can be indexed using the hexagonal structure with $a = 9.426$, $c = 6.0865$ Å and space group $P6_3/m$ (PCPDS-ICDD: 86-1203). Each nanowire is a single crystal and the variation in image contrast in the dark-field TEM image shown in figure 3(b) is due to the local deformation. The corresponding electron diffraction pattern from the nanowires clearly indicates that its growth direction is [0001], top surface (01$\bar{1}$0) and side surfaces (2$\bar{1}\bar{1}$0) (figure 3(c)). A high-resolution transmission electron microscopy (HRTEM) image recorded from the dark-rectangle enclosed area is displayed in figure 3(d), exhibiting its high crystal quality and dislocation-free volume.

3.2. Fluorescence quenching studies on the reverse micelle solution

[Ru(bpy)$_3$]$^{2+}$ used in our experiment (figure 4) is a cationic fluorescent probe which has been used in studies of electronic excitation transport in micelles [27, 28]. In our experiment,
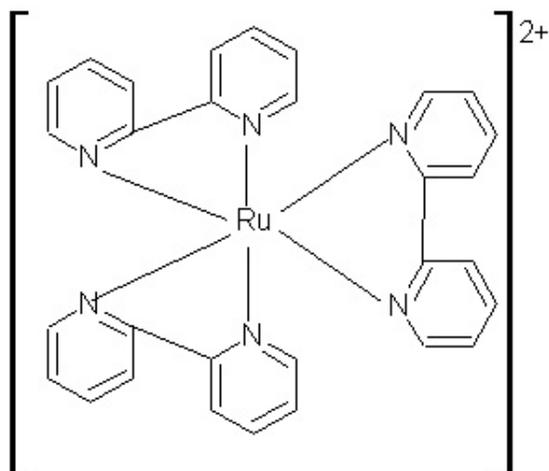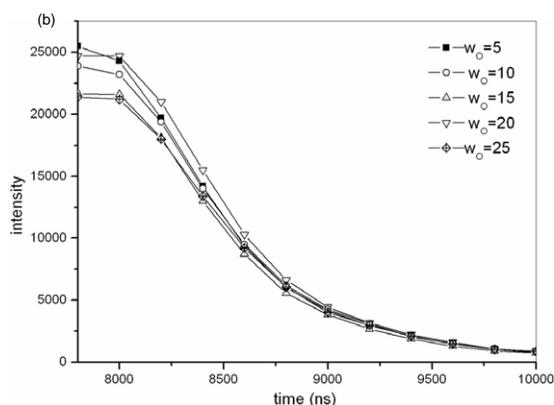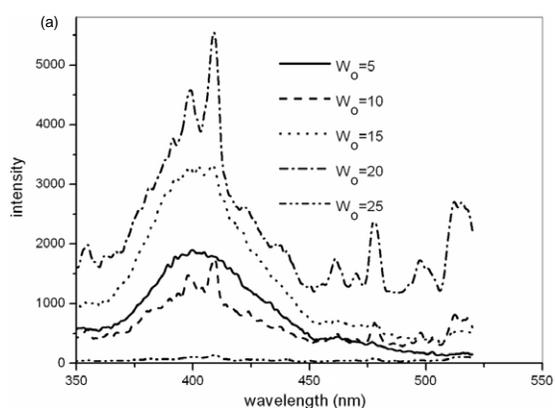
Figure 4. Structure of $Ru(bpy)_3^{2+}$.

Figure 5. Fluorescence spectra and fluorescence intensity decay curve of $[Ru(bpy)_3]^{2+}$ in the system of CTAB/cylcohexane/n-pentanol/water (a). Emission spectra of $Ru(bpy)_3^{2+}$ at different W_0 ($\lambda_{ex} = 272$ nm); (b) fluorescence decay of $Ru(bpy)_3^{2+}$.

the concentration of $[Ru(bpy)_3]^{2+}$ is below 10^{-6}, leading to the molar ratio of H_2O to $[Ru(bpy)_3]^{2+}$ is always $\geqslant 100$. Thus the probability of two $[Ru(bpy)_3]^{2+}$ in the same reverse micelles is low, eliminating the possibility that the two populations represent an equilibrium between two different binding sites within reverse micelles [29].
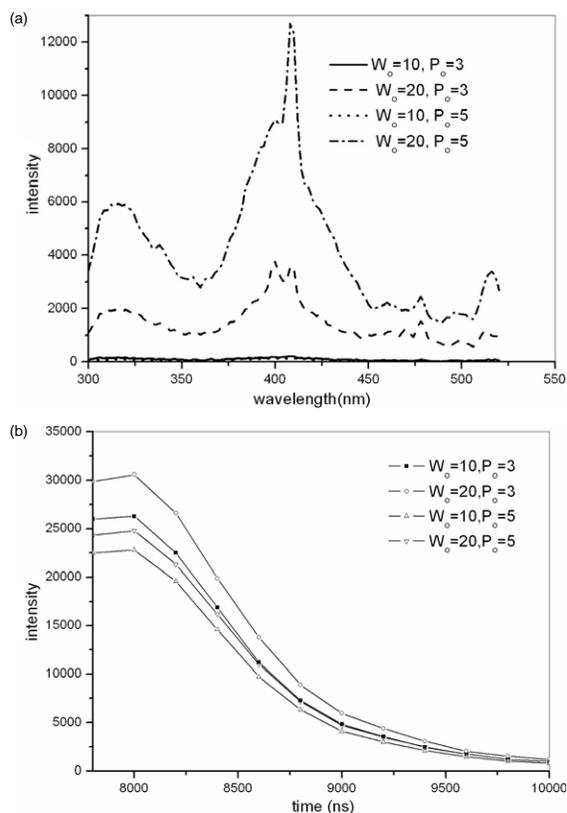
Figure 6. Fluorescence spectra and fluorescence intensity decay curve of $[Ru(bpy)_3]^{2+}$ in the system of CTAB/cylcohexane/n-pentanol/reactant solution (a). Emission spectra of $Ru(bpy)_3^{2+}$ at different W_0 and P_0 ($\lambda_{ex} = 272$ nm); (b) fluorescence decay of $Ru(bpy)_3^{2+}$.

Figures 5 and 6 show the fluorescence spectra and fluorescence intensity decay curve of $[Ru(bpy)_3]^{2+}$ in the different systems. The emission maxima (E_{em}) and lifetimes (τ) of $[Ru(bpy)_3]^{2+}$ in different systems such as CTAB/cyclohexane/n-pentanol/water and CTAB/cyclohexane/n-pentanol/reactant solution are summarized in table 1. The changing E_{em} with increasing W_0 and P_0 values indicates that the probe molecules $[Ru(bpy)_3]^{2+}$ experience an environment somewhere between the interface and core of reverse micelles. The positive charges on both the surfactant headgroups and the probe molecule are expected to repulse $[Ru(bpy)_3]^{2+}$ away from the interface of reverse micelles. In the system of CTAB/cyclohexane/n-pentanol/water, for $W_0 < 10$, biexponential decays are observed, which can also be found in Rack's experiment [29]. The possible explanation by Rack is that at small W_0 the surfactant–probe interactions drive the formation of at least two different-sized nanodroplets in the reverse micelle solution. At larger W_0 values (>10), the single lifetime indicates that the probe is localized near the core of reverse micelles in swollen reverse micelles without the spatial confinement. However, in our experiment, even at large W_0 value (>10) in the system of CTAB/cyclohexane/n-pentanol/reactant solution two separate lifetimes can be observed, suggesting that probe motion is anisotropic, which is hard to reconcile with that in the solution system in the absence of the reactant.

Table 1. Fluorescent parameters in different reaction systems.

Solution	Emission maxima ($\lambda_{\mathrm{em\,max}}$, nm)	Lifetime (ns)	Fluorescence decay equation[a]
CTAB/cyclohexane/n-pentanol/water ($P_0 = 3$)			
$W_0 = 5$	400	64.350 780.986	$I = 5.06 \times 10^8 \exp(-\frac{t}{64.350}) + 5.568 \times 10^8 \exp(-\frac{t}{780.986})$ $R^2 = 0.977$
$W_0 = 10$	409	759.980	$I = 7.807 \times 10^8 \exp(-\frac{t}{759.980})$ $R^2 = 0.977$
$W_0 = 15$	409	759.618	$I = 7.218 \times 10^8 \exp(-\frac{t}{759.618})$ $R^2 = 0.973$
$W_0 = 20$	409	623.578	$I = 9.834 \times 10^9 \exp(-\frac{t}{623.579})$ $R^2 = 0.992$
$W_0 = 25$	410	791.562	$I = 4.695 \times 10^8 \exp(-\frac{t}{791.562})$ $R^2 = 0.974$
CTAB/cyclohexane/n-pentanol/reactant solution			
$W_0 = 10, P_0 = 3$	410	486.974 665.043	$I = 4.122 \times 10^9 \exp(-\frac{t}{665.043}) + 3.123 \times 10^9 \exp(-\frac{t}{486.974})$ $R^2 = 0.976$
$W_0 = 20, P_0 = 3$	408	609.610 680.051	$I = 3.615 \times 10^9 \exp(-\frac{t}{609.610}) + 3.015 \times 10^9 \exp(-\frac{t}{680.051})$ $R^2 = 0.987$
$W_0 = 10, P_0 = 5$	410	587.254 654.279	$I = 3.858 \times 10^9 \exp(-\frac{t}{587.254}) + 3.859 \times 10^9 \exp(-\frac{t}{654.279})$ $R^2 = 0.995$
$W_0 = 20, P_0 = 5$	408	523.962 673.124	$I = 2.231 \times 10^9 \exp(-\frac{t}{523.962}) + 3.515 \times 10^9 \exp(-\frac{t}{673.124})$ $R^2 = 0.985$

[a] All the equations are fitted by software Tablecurve 2D V5.00.

3.3. Growth mechanism of HA nanowires in reverse micelle solution

Quitevis *et al* have presented a 'two-step' model to describe the anisotropy decay of probe molecules sequestered within reverse micelles [14]. In this approach, the anisotropy decays are fitted by a biexponential function. Therefore, it is a manifestation of the motion of the probe species in the reverse micelle solution as the fast motion of probe molecules within the reverse micelles and slow motion of the reverse micelles. The fast and slow motions are assumed to be separable and independent, and the fast motion is modelled as restricted rotational diffusion. In order to describe the spatial restriction of the probe motion within the reverse micelles, the parameter S is introduced so that the total correlation function can be given as follows [14]:

$$I = r_0 \left[\alpha_1 \exp\left(-\frac{t}{\tau_1}\right) + \alpha_2 \exp\left(-\frac{t}{\tau_2}\right) \right] \qquad \alpha_2 > \alpha_1$$
$$\tau_2 > \tau_1 \tag{3}$$

$$C_T(t) = (1 - S^2) \exp\left(-\frac{t}{\tau_{\mathrm{fast}}}\right) + S^2 \exp\left(-\frac{t}{\tau_{\mathrm{slow}}}\right) \tag{4}$$

where the parameter S satisfies the inequalities $0 \leqslant S^2 \leqslant 1$. r_0, α_1 and α_2 are constant; τ_{fast} and τ_{slow} are the correlation times corresponding to fast motion and slow motion.

If the fast motion is isotropic as shown in cyclohexane/n-pentanol/water ($W_0 < 10$) $S = 0$, and if it is completely restricted $|S| = 1$. To apply such a model, the anisotropy decay equations are fitted by the software of Tablecurve 2D V5.00 as shown in table 1. The parameters in the two-step model fitted by computer are shown in table 2. The calculated values of S in the system of CTAB/cyclohexane/n-pentanol/reactant solution are all above zero, suggesting that the probe motion is restricted within the reverse micelles, which is inconstant with the evidence in the system of CTAB/cyclohexane/n-pentanol/water. Especially, at $W_0 = 10$ and $P_0 = 3$, the value of S is equal to unity, indicating the total restricted motion of probe. It is under this condition that the nanowires with high axial ratio are prepared. Unlike in the AOT system [31], probe [Ru(bpy)$_3$]$^{2+}$ will not bond to the surfactant molecule because of their same charges. Then what does entirely restrict the motion of probe within the reverse micelles?

The work by Mann's group [10, 11, 30] on the nanofibres of BaSO$_4$ have shown that the primary surfactant—nanoparticle aggregates are formed in the reverse micelles, which comprise a centrally located amorphous BaSO$_4$/surfactant complex with water-enriched domains at the ends of the shaped aggregate [11]. And the fusion processes of reverse micelles are irreversible, unidirectional and possibly auto-catalytic. Given the envisaged similarities in the CTAB water pool environment, one might hypothesize that the growth process of HA nanowires, within the water pool, may exhibit similar behaviour. In our experiment, the cation surfactant CTAB ionizes completely in the water phase, leading to formation of positive amino headgroups with tetrahedral structure [31]. With the addition of the phosphate reactant, PO$_4^{3-}$ ions, which are also tetrahedral in structure, may bond to one or more headgroups at the interface of the micelles (as shown in figure 7(b)) by electrostatic interaction and structure complementarity. When two reverse micelles involving different reactant ions collide in solution, they are fused by mutual association to form amorphous nuclei. In addition, further fusion processes with other Ca^{2+}-containing and PO$_4^{3-}$-containing reverse micelles will occur as depicted in figure 7. Because of the

Table 2. Two-step model parameters.

Conditions	A	B	a_2	a_1	r_0	S
CTAB/cyclohexane/n-pentanol/water ($P_0 = 3$)						
$W_0 = 5$	5.99E+08	6.61E+08	5.25E−01	4.75E−01	1.14E+09	0.724 435
CTAB/cyclohexane/n-pentanol/reactant solution						
$W_0 = 10$ $P_0 = 3$	3.12E+00	4.12E+09	1.00E+00	7.58E−10	3.12E+00	1
$W_0 = 20$ $P_0 = 3$	3.01E+09	3.61E+09	5.45E−01	4.55E−01	5.53E+09	0.738 397
$W_0 = 10$ $P_0 = 5$	3.86E+09	3.86E+09	5.00E−01	5.00E−01	7.71E+09	0.707 141
$W_0 = 20$ $P_0 = 5$	2.23E+09	3.52E+09	6.12E−01	3.88E−01	3.65E+09	0.782 143

strong affinity for ionized headgroups of CTAB and amorphous nuclei mentioned above, the CTAB molecules at the central region of reverse micelles are immobilized. By comparison, the CTAB molecules at the ends of reverse micelles can exchange with other isolated surfactant molecules in the reverse micelle solution, leading to fluidity of the reverse micelle at the end of it. As a result, the uni-directional fusions of reverse micelles are favoured by this kind of shape fluctuation. However, the entire restriction of the probe's motion cannot yet be interpreted by this. In our experiments, the positive ions coming from the ionized headgroups of CTAB inhabit the interface of reverse micelles. At the same time, it is supposed that the negative ions coming from the amorphous nucleus might dispose at the ends of the nucleus. And the presence of the different charges on the surfaces of the reverse micelles and amorphous nucleus leads to the formation of an electrostatic field (as shown in figures 7(a) and 8), which directs the aggregation of the crystalline HA building blocks along one principal axis. In support of the existence of this electrostatic field, we note that the motion of the probe molecule $[Ru(bpy)_3]^{2+}$ is anisotropic in the presence of reactant solution. Contrastively, the probe motion is isotropic in the absence of reactant solution because only one decay lifetime can be observed. It could therefore be expected that the motion of $[Ru(bpy)_3]^{2+}$ is restricted to some extent in this electrostatic field. In particular, when $W_0 = 10$ and $P_0 = 3$, $[Ru(bpy)_3]^{2+}$ is entirely bounded to the surface of the amorphous nucleus, leading to $|S| = 1$ (as shown in figure 8). In principle, the electrostatic field should be tuneable by the density of the charges on the surface of the reverse micelles and this might explain why the additions of co-surfactant give rise to the formation of various morphologies of the final products as demonstrated in our previous paper [25]. The intervention of the co-surfactant molecules in the interface of reverse micelles should decrease the density of positive ions at the interface and this will weaken the intensity of the electrostatic field. As a result, the surfactant molecule will lose the morphology control of the HA nanowire with the increase of co-surfactant. Furthermore, various authors have proposed the hypothesis that in a biological system intrinsic electric fields take over control of biomimetic growth and self-assembly of fluorapatite aggregates [32–34]. This means that the individual 'crystals' contain a permanent dipole during apatite formation under *in vivo*

Table 3. The saturated vapour pressures of various components at 120 °C.

Components	Saturated vapour pressures (kPa)
Cyclohexane	362.70
n-pentanol	80.89
Water	270.02

or biomimetic conditions [32], which is consistent with the assumption of electrostatic field in our experiment. It is also because of the electrostatic field that the fusion between reverse micelles prefers to operate in one direction. The uni-directional fusion of reverse micelles provides the possibility for crystal growth along one direction and would be responsible for the long nanowires observed in figures 2 and 3. However, many factors can affect the stability of the inner electrostatic field such as the content of water, n-pentanol, pH, reaction temperature and time. We have discussed these effects in detail in our previous papers [12, 24, 25]. In addition, based on the results of a time-resolved fluorescence quenching experiment conducted at room temperature, it therefore could be expected that reverse micelles play a major role in growth guidance at the nucleation stage. However, solvothermal reactions have to be performed in the sealed and opaque Teflon autoclave; the invisible reaction process makes the growth mechanism of nanowires at higher temperature ambiguous. Although the exact process of the crystal growth is not yet clear, the experimental results indicate that the interaction between the surfactant molecules and the nucleus is still firm even at higher temperature and pressure under the condition of $W_0 = 10$ and $P_0 = 3$ as the nanowires grow defect-free up to several micrometres in length.

3.4. The reaction pressure in solvothermal synthesis

As a matter of safety, the pressures generated in the sealed autoclave should always be estimated. The equations necessary for doing so go far beyond the ideal gas law and are outlined in the review by Rajamathi and Seshadri [35]. The equation takes the form

$$P = \left[\frac{RT}{V_m - b} \right] - \left[\frac{a}{V_m^2 + 2bV_m - b^2} \right]. \tag{5}$$
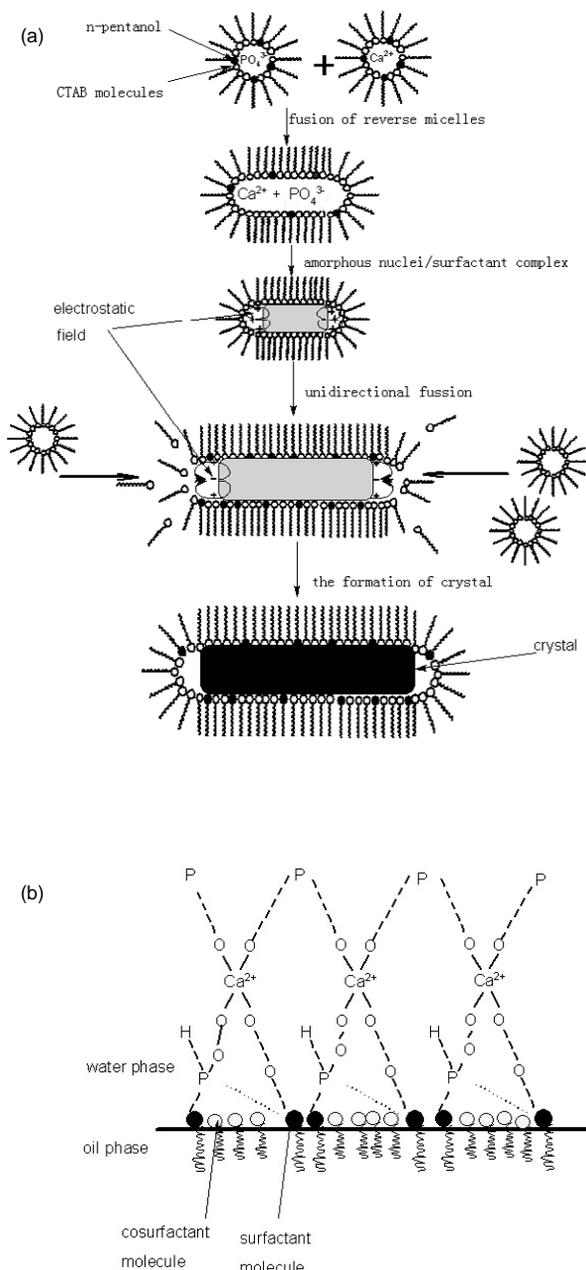
(a)

(b)

Figure 7. (a) Illustration of the formation of monetite nanoparticles formed in CTAB/water/n-pentanol/cyclohexane/reactant reverse micelle solution. (b) Enlarged illustration of the interaction between the crystal and the surfactant molecule at the inner side interface.

The parameters a and b are given by

$$a = \frac{0.457\,24R^2T_C^2\left[1 + f_\omega(1 - T_r^{\frac{1}{2}})\right]^2}{P_C}$$

$$b = \frac{0.007\,78RT_C}{P_C}$$

$$f_\omega = 0.374\,64 + 1.542\,26\omega - 0.269\,92\omega^2$$

where p indicates the pressures generated in the autoclaves; V_m is the molar volume of the liquid phase in the autoclaves;
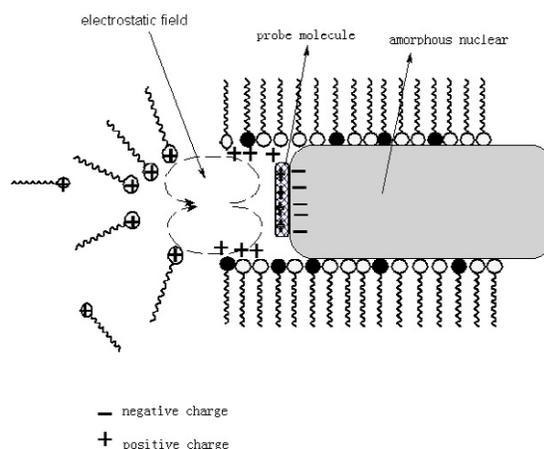

Figure 8. Enlarged illustration for the motion of probe molecules within the reverse micelles. At $W_0 = 10$ and $P_0 = 3$, the probe molecule is bound to the amorphous nuclear surface.

T is the reaction time; T_c and P_c are the critical temperature and pressure of solvents; acentric factor ω can be consulted in reference [36] and $R = 8.3144$ J mol^{-1} K^{-1}. Table 3 shows the saturated vapour pressure of various components at $120\,°C$. For a filling fraction of 0.95 of cyclohexane, 0.03 of n-pentanol and 0.02 of water phase in the autoclave, it is reasonable to ignore the contributions of n-pentanol and water to the pressure and volume of the overall reaction. This means that, at $120\,°C$, V_m, T_C and P_C of the reaction system are 0.108 m^3 mol, 553.45 K and 4073.265 kPa, which are approximately equal to cyclohexane, respectively. As a result, the pressure generated in the autoclave is approximately 324 kPa, which is below the saturated vapour pressure of cyclohexane. It is suggested that in this case the solvothermal synthesis is conducted under gentle conditions without the intense convection of fluid and the intense shearing stress. These stable conditions favour the growth of long and uniform nanowires. Moreover, our previous experiments indicate that this presumption proceeds with high fidelity as the long nanobundles consisting of several parallel nanowires were formed at $130\,°C$ in the autoclave. If the nanomaterials were prepared under unstable conditions, the fibre formation and the parallel fusion of nanowires would all be suppressed. This is in agreement with the results of Antonietti's experiments that no BaCrO$_4$ fibre bundles or cones were obtained if the solution was stirred continuously [37].

4. Conclusion

In conclusion, we report the solvothermal synthesis of hydroxyapatite with high axial ratio in the present paper, and a generalized mechanism for the growth of nanowires in reverse micelles is described.

Firstly, uniform hydroxyapatite (HA) nanowires of width 60 nm and length 1 μm are synthesized by solvothermal synthesis in our experiment.

Secondly, the results of the time-resolved fluorescence quenching technique indicate that the formation of amorphous nuclear/surfactant complex and the electrostatic field within the reverse micelles lead to the orientation and irreversible merging of reverse micelles, which ensure the one-dimensional growth of the nanowires.

Thirdly, by estimating the pressure generated within the autoclave, it is suggested that in our experiments the solvothermal synthesis is conducted under gentle conditions without the intense convection of fluid and the intense shearing stress. These stable conditions favour the growth of long and uniform nanowires.

The ability to generate high axial ratio and well crystallized hydroxyapatite by solvothermal synthesis provides a new approach for large-scale synthesis of hydroxyapatite nanowires, which is expected to have significantly improved mechanical properties for biomedical applications.

Acknowledgments

References

[1] Wang X D, Summers C J and Wang Z L 2004 *Nano Lett.* **4** 423
[2] Dai Z R, Pan Z W and Wang Z L 2003 *Adv. Funct. Mater.* **13** 9
[3] Li Y, Meng G W, Zhang L D, Zhang L D and Philip F 2000 *Appl. Phys. Lett.* **76** 2011
[4] Hopwood J D and Mann S 1997 *Chem. Mater.* **9** 1819
[5] Qi L, Ma J, Cheng H and Zhao Z 1997 *J. Phys. Chem.* B **101** 3460
[6] Rees G D, Evans-Goning R, Hammond S and Robinson B H 1999 *Langmuir* **15** 1993
[7] Faeder J and Ladanyi B M 2000 *J. Phys. Chem.* B **104** 1033
[8] Thomas J K 1980 *Chem. Rev.* **80** 283
[9] Sarda S, Heughebaert M and Lebugle A 1999 *Chem. Mater.* **11** 2722
[10] Mann S, Davis S A, Hall S R, Li M, Rhodes K, Shenton W, Vancher S and Zhang B J 2000 *J. Chem. Soc., Dalton Trans.* **21** 3753
[11] Hopwood J D and Mann S 1997 *Chem. Mater.* **9** 1819
[12] Lai C *et al* 2005 *Mater. Lett.* **59** 210
[13] Das R K and Chaudhuri A 1999 *Langmuir* **15** 8871
[14] Quitevis E L, Marcus A H and Fayer M D 1993 *J. Phys. Chem.* **97** 5762
[15] Rack J J, Mccleskey T M and Birnhaum E R 2002 *J. Phys. Chem.* B **106** 632
[16] Sáez M, Abuin E A and Lissi E A 1989 *Langmuir* **5** 942
[17] Kondo H, Miwa I and Sunamoto J 1982 *J. Phys. Chem.* **86** 4826
[18] Corbeil E M and Levinger N E 2003 *Langmuir* **19** 7264
[19] Giachelli C M 1999 *Am. J. Pathol.* **154** 671
[20] Hughes W L and Wang Z L 2005 *Appl. Phys. Lett.* **86** 043106-1
[21] Mavis B and Tas A C 2000 *J. Am. Ceram. Soc.* **83** 989
[22] Weng W and Bapsta J L 1999 *J. Am. Ceram. Soc.* **82** 27
[23] Suchanek W and Yoshimura M 1998 *J. Mater. Res.* **13** 94
[24] Lai C, Tang S Q, Wang Y J, Wei K and Zhang S Y 2005 *Synth. React. Inorg. Met.* **9** 717
[25] Wang Y J, Lai C, Wei K and Tang S Q 2005 *Mater. Lett.* **59** 1098
[26] Foreman T K, Sobol W M and Whitten D G 1981 *J. Am. Chem. Soc.* **103** 5333
[27] Szulbinski W S and Kincaid J R 1998 *Inorg. Chem.* **37** 859
[28] Bhuiyan A A and Kincaid J R 1998 *Inorg. Chem.* **37** 2525
[29] Rack J J, McCleskey T M and Birnabaum E R 2002 *J. Phys. Chem.* B **106** 632
[30] Li M and Mann S 2000 *Langmuir* **16** 7088
[31] Li Y, Li Y D, Deng Z X, Zhuang J and Sun X M 2001 *Int. J. Inorg. Mater.* **3** 633
[32] Busch S, Dolhaine H, DuChesne A, Heinz S, Hochrein O, Laeri F, Podebrad O, Vietze U, Weiland T and Kniep R 1999 Biomimetic morphogenesis of fluorapatite-gelatin composites: fractal growth, the question of intrinsic electric fields, core/shell assemblies, hollow spheres and reorganization of denatured collagen *Eur. J. Inorg. Chem.* **1999** 1643–53
[33] Kniep R and Busch S 1996 *Angew. Chem.* **108** 2788
[34] Kniep R and Busch S 1996 *Angew. Chem. Int. Edn Engl.* **35** 2624
[35] Rajamathi M and Seshadri R 2002 *Curr. Opin. Solid State Mater.* **6** 337
[36] Twu C H, Coon J E and Cunningham J R 1994 *Fluid. Phase Equilib.* **96** 19
[37] Yu S H, Cölfen H and Antonietti M 2002 *Chem. Eur. J.* **8** 2937